ELSEVIER

Earth and Planetary Science Letters 197 (2002) 35–50

EPSL

www.elsevier.com/locate/epsl

Relationship between the early Kerguelen plume and continental flood basalts of the paleo-Eastern Gondwanan margins

Stephanie Ingle [a,*], Dominique Weis [a,1], James S. Scoates [a], Frederick A. Frey [b]

[a] *Département des Sciences de la Terre et de l'Environnement, Université Libre de Bruxelles, P.O. Box 160/02, Ave. F.D. Roosevelt 50, B-1050 Brussels, Belgium*

[b] *Department of Earth, Atmospheric and Planetary Sciences, Massachusetts Institute of Technology, Building 54-1226, Cambridge, MA 02139, USA*

Received 4 June 2001; received in revised form 10 December 2001; accepted 10 January 2002

Abstract

Cretaceous basalts recovered during Ocean Drilling Program Leg 183 at Site 1137 on the Kerguelen Plateau show remarkable geochemical similarities to Cretaceous continental tholeiites located on the continental margins of eastern India (Rajmahal Traps) and southwestern Australia (Bunbury basalt). Major and trace element and Sr–Nd–Pb isotopic compositions of the Site 1137 basalts are consistent with assimilation of Gondwanan continental crust (from 5 to 7%) by Kerguelen plume-derived magmas. In light of the requirement for crustal contamination of the Kerguelen Plateau basalts, we re-examine the early tectonic environment of the initial Kerguelen plume head. Although a causal role of the Kerguelen plume in the breakup of Eastern Gondwana cannot be ascertained, we demonstrate the need for the presence of the Kerguelen plume early during continental rifting. Activity resulting from interactions by the newly formed Indian and Australian continental margins and the Kerguelen plume may have resulted in stranded fragments of continental crust, isolated at shallow levels in the Indian Ocean lithosphere.

Keywords: Kerguelen Plateau; ODP Site 1137; continental crust; enrichment; mantle; Indian Ocean

1. Introduction

Oceanic plateaus result from voluminous magmatic activity over a (typically) short period of geological time (10^6 years) and create lithosphere that is as much as four times the thickness of normal oceanic lithosphere [1]. The Cretaceous Kerguelen Plateau in the southern Indian Ocean is the second largest oceanic plateau [1] and has been interpreted as the surface manifestation of Kerguelen mantle plume activity during the opening of the Indian Ocean between India and Australia–Antarctica [2,3]. Ocean Drilling Program

* Corresponding author.
Tel.: +32-2-650-22.40; Fax: 32-2-650-37.48.
E-mail address: single@ulb.ac.be (S. Ingle).

[1] Directeur de Recherches, F.N.R.S.

0012-821X/02/$ – see front matter
PII: S0012-821X(02)00473-9

(ODP) Legs 119, 120 and 183 have sampled Kerguelen Plateau crust. Contamination of the recovered basalts by continental lithosphere was proposed to explain extreme isotopic and trace element features at Site 738 (Leg 119) on the southernmost edge of the Kerguelen Plateau (Fig. 1 [4]). Moreover, drilling during Leg 183 recovered rocks of unequivocal continental origin (i.e., garnet–biotite gneiss) from fluvial units intercalated with basalts at Site 1137 on Elan Bank, a western salient protruding from between the Southern and Central Kerguelen Plateau (Fig. 1; e.g., [5]). Basaltic lavas recovered at Site 1137 erupted during the earlier stages of Kerguelen Plateau formation, at ~109 Ma (Fig. 1 [6]), within the range of volcanism on the Southern Kerguelen Plateau (119–109 Ma [7,8]) and prior to that of the Central Kerguelen Plateau (100–85 Ma [7,8]). Site 1137 basalts are, therefore, critical to deciphering the early magmatic history of the Kerguelen plume system, its mantle sources and the possible continental contaminants.

Early Cretaceous volcanism in proximity to the Kerguelen Plateau also occurred along the paleo-Eastern Gondwanan margins of Australia and India. The Bunbury basalt of Western Australia records two periods of geochemically distinct continental basalt outpouring at 132 Ma (Casuarina Group [8,9]) and 123 Ma (Gosselin Group [9]). The Rajmahal Traps of eastern India erupted at

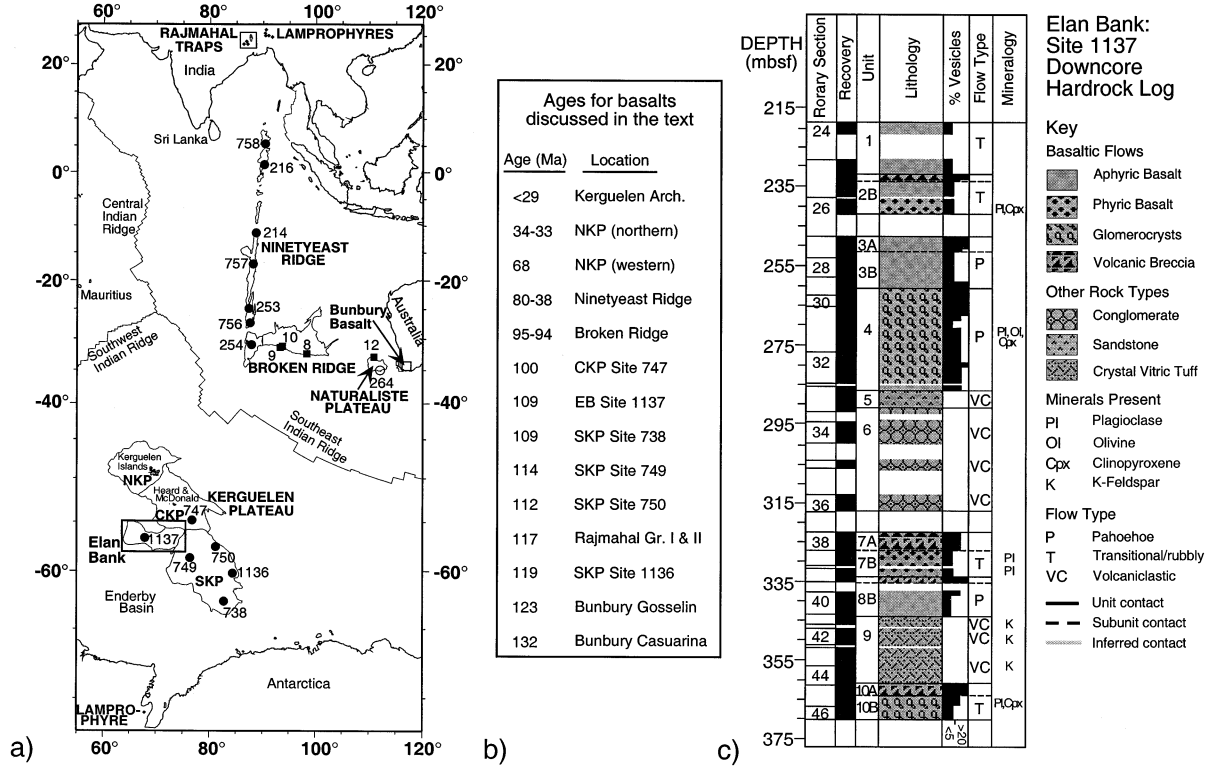

Fig. 1. (a) Physiographic map depicting major volcanic features of the Indian Ocean and surrounding continents [56]. ODP basement sites are marked by filled circles and dredge locations are marked by filled squares. Rectangles delineate the Elan Bank, Kerguelen Plateau (location of Site 1137), the Bunbury basalt (southwestern Australia) and the Rajmahal Traps (eastern India). The four main physiographic provinces of the Kerguelen Plateau are labeled: SKP (Southern Kerguelen Plateau), CKP (Central Kerguelen Plateau), Elan Bank and the NKP (Northern Kerguelen Plateau). (b) Summary of approximate ages for basalts discussed in the text. Age data sources are as follows: Bunbury [8,9], Rajmahal [10,11], SKP Site 1136 and CKP Site 1138, NKP and Broken Ridge [7], SKP Sites 738, 749 and 750 [8], Site 1137 [6], Kerguelen Archipelago [57–59]. (c) Site 1137 downcore hardrock log (mbsf is meters below sea floor) from [17]. The depth, section number, recovery, unit number, general lithology, % vesicularity, flow type and dominant mineralogy (for phyric rocks) are depicted.

117 Ma [10–12] and have also been divided into two groups on the basis of geochemistry (Groups I and II [13]). Geochemical similarities between the Rajmahal Traps and Bunbury basalt and basalts of the Kerguelen Plateau have been noted previously [9] and the volcanism attributed to impingement of the Kerguelen plume beneath the lithosphere of Eastern Gondwana. Most workers have inferred involvement of heat derived from the plume, rather than substance in their petrogenesis [9,11,14].

Recent wide-angle seismic profiling has shown that the crustal structure of Elan Bank has geophysical characteristics similar to continental crust [15,16]. Although it is currently submerged, basement Units 1–4, 7, 8 and 10 are subaerially erupted basalt flows with brecciated upper margins and Units 5, 6 and 9 are fluvial volcaniclastic deposits (Fig. 1 [17]). A surprising result at Site 1137 was the recovery of a volcaniclastic polymict conglomerate containing pebble-sized clasts of variable lithologies, including some of continental derivation [5,18,19]. In this paper, we expand upon an initial study of the basalts [20] with a much more detailed sampling and thorough geochemical investigation to characterize and quantify the mantle sources and continental contaminants in early Kerguelen Plateau basalts. In light of a comparison with basalts of the paleo-Eastern Gondwanan margins, we re-examine existing models for the timing and emplacement mechanism of the Kerguelen plume, which range from post-continental breakup and rapid initial eruption rates (e.g., [5,21]) to pre-continental breakup and long-term incubation of the Kerguelen plume beneath Gondwanan lithosphere (e.g., [22,23]). Our results support the presence of the Kerguelen plume coincident with early separation of eastern Gondwana and suggest that the Kerguelen plume may have played an active role in the isolation of continental material at shallow levels within the incipient Indian Ocean crust.

2. Analytical techniques

The freshest core samples were selected from each basalt flow unit. To remove surficial contamination by the drill bit and saws, the exterior of each sample was sanded with silicon carbide paper and rinsed using an ultrasonic bath of ultrapure water. Chips from each coarse-crushed sample were hand-picked under a binocular microscope to remove visibly altered pieces; remaining chips were powdered in an agate swing mill. Rock powders were analyzed by X-ray fluorescence (XRF) methods (University of Massachusetts) and instrumental neutron activation analysis (INAA; Massachusetts Institute of Technology) for major and trace elements (Table 1). All XRF data reported for major elements are averages of duplicate analyses. Details of accuracy and precision for both methods are reported by [24].

Representative samples from each flow unit were analyzed for radiogenic (Sr, Nd and Pb) isotopic compositions (Table 2). To remove the effects of post-magmatic alteration, between 250 and 300 mg of rock powder was placed in a Teflon vial and leached with 6 N HCl following 'cold' leaching methods [25,26]. On average, samples were leached eight times (until the leachate was clear) and lost $\sim$30 wt%. The reproducibility of the leaching and the effectiveness at removing secondary alteration minerals can be assessed by our duplicate analysis of 31R-1-5–10 (Table 2). Chemical procedures for dissolution follow [27] and [26]. All radiogenic isotopic compositions were determined with a VG Elemental Sector 54 multicollector thermal ionization mass spectrometer at the Université Libre de Bruxelles. Sr and Nd isotopic compositions were measured on single Ta and triple Re–Ta filaments, respectively, in dynamic mode. Sr isotopic ratios were normalized to $^{86}Sr/^{88}Sr = 0.1184$ and Nd isotopic data were normalized using $^{146}Nd/^{144}Nd = 0.7219$. The average $^{87}Sr/^{86}Sr$ value for the NBS 987 Sr standard was 0.710279 ± 7 (2σ) on the basis of 65 analyses. The average Nd standard (Rennes [28]) $^{143}Nd/^{144}Nd$ value was 0.511964 ± 11 (2σ) for 75 runs. Pb isotopic ratios were measured on single Re filaments using the H_3PO_4–silica gel technique. All Pb isotopic ratios were corrected by 1.2‰ per atomic mass unit to account for mass fractionation on the filament, based on 80 analyses

Table 1
Major element oxide (wt%) and trace element concentration (ppm) data for Site 1137 basaltic rocks

Core	24R-2	25R-1	25R-2	25R-2	25R-3	25R-5	25R-7	26R-1	26R-1	26R-2	26R-3	27R-4	28R-3	29R-1	29R-2	30R-2	31R-3
Interval	10–17	64–72	46–53	119–126	72–79	52–60	90–98	31–43	143–146	17–23	51–60	57–63	123–128	30–37	31–38	21–26	5–10
Depth[a]	220.39	229.04	230.3	231.03	231.94	234.38	237.08	238.31	239.43	239.65	241.45	252.49	256.62	257.5	258.77	263.45	269.65
Group	Upper																
	Unit 1	Unit 1	Unit 1	Unit 1	Unit 1	Unit 2	Unit 2	Unit 2	Unit 2	Unit 2	Unit 2	Unit 3	Unit 3	Unit 3	Unit 3	Unit 4	Unit 4
SiO_2	51.45	52.27	52.70	52.10	50.93	53.87	52.30	52.83	52.87	53.15	51.89	51.51	52.65	51.15	50.65	52.20	52.20
TiO_2	2.36	2.33	2.33	2.39	2.47	2.51	2.45	2.34	2.11	2.54	2.66	2.58	2.54	2.66	2.69	2.04	2.09
Al_2O_3	15.09	14.69	14.46	14.50	15.32	14.11	14.79	14.40	14.66	14.12	14.64	15.10	14.41	15.20	15.28	15.62	16.19
Fe_2O_3	10.79	10.88	11.08	11.20	10.79	11.76	10.64	10.99	10.27	11.26	11.52	11.48	11.46	11.02	11.55	9.99	9.83
MnO	0.10	0.14	0.15	0.14	0.12	0.10	0.11	0.15	0.15	0.16	0.15	0.11	0.15	0.12	0.12	0.08	0.11
MgO	5.70	5.86	5.84	5.91	6.23	5.54	5.53	5.79	6.11	5.15	5.43	6.54	5.62	5.77	6.59	6.51	6.02
CaO	8.97	9.29	9.23	9.26	9.24	5.72	8.99	9.20	9.59	8.75	7.35	7.94	8.98	9.08	7.43	7.87	9.31
Na_2O	3.74	3.00	2.97	2.97	3.35	3.23	3.11	3.04	3.04	3.18	3.38	3.21	3.08	3.29	3.50	3.22	3.01
K_2O	1.02	0.78	0.84	0.75	0.70	2.78	0.98	0.96	0.92	1.13	2.24	1.30	0.87	0.77	1.69	2.13	1.07
P_2O_5	0.34	0.34	0.33	0.33	0.35	0.37	0.35	0.34	0.30	0.38	0.40	0.38	0.37	0.39	0.39	0.27	0.28
Total	99.56	99.58	99.93	99.55	99.50	99.99	99.24	100.04	100.01	99.82	99.66	100.15	100.13	99.45	99.89	99.93	100.11
LOI[b]	4.82	2.85	2.37	2.88	4.28	4.46	3.62	1.80	1.53	0.96	3.43	6.22	2.73	5.03	5.05	7.94	4.42
Mg#[c]	0.51	0.52	0.51	0.51	0.53	0.48	0.51	0.51	0.54	0.48	0.48	0.53	0.49	0.51	0.53	0.56	0.55
AI[d]	0.15	−1.15	−1.26	−1.13	−0.37	0.50	−0.84	−1.12	−1.18	−0.93	0.85	−0.12	−1.10	−0.44	0.88	0.47	−0.80
Sc[e]	25.8	26.2	25.7	26.2	–	24.8	26.2	26.3	26.7	25.4	25.9	26	25.9	27.4	–	–	23.5
V	–	205	202	211	–	215	216	207	193	212	–	227	209	226	–	–	204
Cr	97	96	88	82	–	51	85	86	100	48	50	63	60	63	–	–	146
Ni	–	22	21	20	–	17	20	21	21	15	–	24	21	23	–	–	40
Zn	–	112	110	113	–	118	113	111	101	115	–	122	115	122	–	–	97
Ga	–	22	22	22	–	22	23	22	22	22	–	23	23	24	–	–	22
Rb	–	6	12	8.5	–	31.8	12.2	12.9	12.3	20.2	–	17.9	16	6.6	–	–	11
Sr	–	536	530	537	–	405	536	520	529	508	–	523	532	566	–	–	540
Y	–	26.9	26.9	26.3	–	28	26.5	27.4	24.4	29.4	–	29.1	28.8	30.1	–	–	23.1
Zr	–	210	208	212	–	229	216	211	185	233	–	233	232	241	–	–	173
Nb	–	14.9	14.6	15	–	16.3	15	14.9	12.8	16.3	–	16.3	16	16.8	–	–	12.4
Ba	–	296	310	305	–	296	322	325	301	364	–	294	333	340	–	–	202
La	19.7	20.5	20.5	19.8	–	22.2	20.2	21.0	18.5	23.7	23.6	22.3	22.5	23.5	–	–	16.5
Hf	4.73	5.25	5.16	5.29	–	5.52	5.03	4.77	4.36	5.04	5.7	5.53	5.47	5.52	–	–	3.96
Ta	0.79	0.88	0.86	0.76	–	0.86	0.81	0.82	0.74	0.9	0.94	0.83	0.85	0.94	–	–	0.63
Ce	44.7	49.9	48.1	48	–	53.8	47.9	51.1	43.8	54.1	56.5	52.6	54.2	56.7	–	–	39.4
Nd	25.7	28.8	26.7	28.4	–	31	27.9	28.2	24.6	31	31.1	29.4	29.4	31	–	–	23.4
Sm	6.27	6.56	6.26	6.39	–	6.8	6.41	6.71	5.77	7.03	7.18	6.89	7.07	7.27	–	–	5.41
Eu	2.11	2.15	2.15	2.13	–	2.24	2.21	2.17	2.03	2.32	2.34	2.28	2.32	2.42	–	–	1.89
Tb	0.91	0.89	1.03	0.86	–	1.08	1	1.21	0.81	0.99	1.07	0.95	0.98	1.09	–	–	0.74
Yb	2	2.19	2.22	2.09	–	2.32	2.2	2.23	1.95	2.37	2.59	2.26	2.32	2.38	–	–	1.85
Lu	0.3	0.31	0.31	0.3	–	0.32	0.32	0.33	0.28	0.36	0.34	0.35	0.33	0.38	–	–	0.27
Th	2.09	2.9	2.16	2.4	–	2.5	2.27	2.22	2	2.56	2.67	2.36	2.4	2.54	–	–	1.64

Table 1 (*Continued*)

Core	31R-3	31R-6	31R-7	32R-6	33R-1	37R-3	38R-1	38R-3	38R-4	39R-1	39R-2	40R-3	41R-1	41R-1	45R-3	46R-1	46R-2	46R-3
Interval	85–90	24–30	125–130	66–71	53–60	12–20	73–78	63–68	71–77	101–108	50–54	117–124	3–10	67–78	57–63	51–56	7–15	12–18
Depth[a]	270.45	273.63	276.14	282.88	286.03	324.84	328.23	329.95	331.39	333.21	334.00	340.62	343.03	343.67	364.84	367.51	368.54	369.92
Group	Upper, cont.					Lower												
	Unit 4	Unit 4	Unit 4	Unit 4	Unit 4	Unit 7	Unit 7	Unit 7	Unit 7	Unit 7	Unit 7	Unit 8	Unit 8	Unit 8	Unit 10	Unit 10	Unit 10	Unit 10
SiO_2	51.53	50.40	53.02	50.84	50.40	51.61	51.05	51.40	52.97	52.61	50.46	53.19	51.83	49.06	49.90	51.41	51.69	51.85
TiO_2	2.23	2.19	2.06	2.53	2.58	2.09	2.19	2.12	2.04	2.06	2.21	2.02	2.13	2.47	2.60	2.61	2.63	2.76
Al_2O_3	16.39	16.62	15.62	15.61	16.06	16.25	16.73	15.91	15.30	15.50	16.40	15.23	15.99	18.69	17.27	15.94	15.45	14.83
Fe_2O_3	10.02	10.09	10.04	11.34	11.50	10.98	10.64	10.78	10.45	10.78	11.26	10.23	11.02	12.32	10.85	11.02	11.24	11.86
MnO	0.14	0.18	0.11	0.14	0.14	0.30	0.24	0.14	0.17	0.17	0.17	0.13	0.21	0.28	0.17	0.15	0.15	0.16
MgO	5.79	6.58	7.07	5.83	5.78	6.99	6.16	5.79	5.46	5.50	6.81	5.16	5.59	4.01	4.86	4.90	4.45	4.77
CaO	9.94	8.69	4.62	9.20	9.23	4.90	7.49	9.40	9.41	9.43	7.47	8.82	9.33	7.79	8.38	9.68	9.41	9.27
Na_2O	3.08	3.24	3.13	3.29	3.30	3.15	3.52	3.10	3.05	3.09	3.49	2.67	3.11	3.28	3.07	3.33	3.43	3.24
K_2O	0.62	1.37	3.38	0.71	0.56	3.09	1.70	0.59	0.61	0.62	1.37	1.52	0.61	0.73	1.56	0.64	0.78	0.78
P_2O_5	0.32	0.30	0.29	0.36	0.37	0.29	0.31	0.30	0.29	0.29	0.31	0.28	0.30	0.35	0.37	0.35	0.37	0.38
Total	100.05	99.66	99.34	99.85	99.92	99.65	100.03	99.53	99.75	100.05	99.95	99.25	100.12	98.98	99.03	100.03	99.60	99.90
LOI[b]	3.66	3.79	7.97	4.74	4.96	10.94	4.57	4.48	1.92	2.37	6.00	2.37	4.19	8.54	3.76	3.04	2.15	2.36
Mg#[c]	0.53	0.56	0.58	0.50	0.50	0.56	0.53	0.52	0.51	0.50	0.55	0.50	0.50	0.39	0.47	0.47	0.44	0.44
AI[d]	−0.94	0.39	1.32	−0.38	−0.36	1.57	0.76	−0.90	−1.51	−1.33	0.62	−1.06	−1.03	−0.29	0.6	−0.62	−0.49	−0.73
Sc[e]	24.8	24.4	–	25.4	25.5	–	26	25.5	25.3	25.2	–	25.3	25.6	–	23.3	24.6	24.4	25.9
V	202	–	–	225	233	–	–	–	200	198	230	202	208	246	–	191	189	196
Cr	141	153	–	106	105	–	101	93	95	95	–	90	90	–	133	144	139	148
Ni	37	–	–	37	39	–	–	–	29	28	32	27	28	35	–	54	53	52
Zn	103	–	–	120	122	–	–	–	111	111	116	107	114	131	–	114	116	121
Ga	23	–	–	23	24	–	–	–	21	22	22	21	22	26	–	23	23	23
Rb	11.2	–	–	12.7	8.6	–	–	–	16.5	16.7	23.6	36.1	9.3	7.7	–	14.2	19.9	19.3
Sr	573	–	–	545	560	–	–	–	485	484	477	456	483	562	–	494	478	455
Y	25	–	–	28	27.9	–	–	–	27.3	27.8	26.6	27.7	28.8	27.2	–	30.6	31	32.2
Zr	189	–	–	216	219	–	–	–	190	192	199	193	201	231	–	204	214	221
Nb	13.6	–	–	15.9	15.8	–	–	–	13.2	13.3	13.8	12.9	13.6	15.6	–	14.7	15.2	15.9
Ba	227	–	–	256	258	–	–	–	268	260	450	288	296	266	–	304	318	325
La	18.0	17.5	–	20.0	20.2	–	21.3	20.4	20.2	20.6	–	21.0	21.0	–	22.0	20.7	21.3	22.7
Hf	4.41	4.48	–	4.79	4.88	–	4.46	4.61	4.57	4.56	–	4.64	4.82	–	4.94	4.96	5.15	5.4
Ta	0.77	0.76	–	0.95	0.87	–	0.82	0.7	0.7	0.7	–	0.76	0.75	–	0.87	0.81	0.85	0.85
Ce	43.7	41.1	–	49.4	48.1	–	47.6	47.8	47.7	47.9	–	49.8	50.5	–	50.8	49.5	52.1	54.1
Nd	25.5	24.5	–	27.6	28.2	–	25.6	27.1	27.1	26.9	–	26.5	26.6	–	29.9	28.9	29.3	29.7
Sm	6.02	5.71	–	6.63	6.54	–	5.95	6.1	6.03	6.17	–	6.34	6.23	–	6.7	6.72	6.9	7.32
Eu	2.02	2.03	–	2.16	2.2	–	1.94	2.04	2.03	2.02	–	2.00	2.04	–	2.21	2.22	2.27	2.3
Tb	0.97	0.83	–	0.88	0.98	–	0.92	0.94	0.9	0.91	–	0.96	1.0	–	1.05	1.06	1.03	1.17
Yb	2.01	1.91	–	2.1	1.93	–	2.02	2.1	2.04	2.46	–	2.21	2.64	–	2.32	2.44	2.66	2.71
Lu	0.29	0.3	–	0.32	0.29	–	0.32	0.34	0.33	0.3	–	0.35	0.31	–	0.36	0.39	0.34	0.39
Th	2.12	1.82	–	2.08	2.52	–	2.93	3.09	3.28	3.23	–	3.65	3.7	–	2.68	2.72	3.02	2.87

[a] Depth is reported in meters below sea floor.

[b] LOI is wt% loss-on-ignition at 1000°C.

[c] Mg# = (wt% MgO/40.311)/[(wt% MgO/40.311)+(wt% FeO/71.846)], assuming all Fe as Fe^{+2} ($FeO = 0.8998 \times Fe_2O_3$).

[d] Alkali index, calculated from [29] as $AI = (Na_2O+K_2O)-(SiO_2 \times 0.37–14.43)$; tholeiitic series rocks have negative values and alkalic series have positive values.

[e] Sc, Hf, Ta, Th and the rare earth elements are by INAA methods; all other elements are by XRF methods.

of NBS 981 Pb standard run at a temperature between 1090°C and 1200°C. Samples were run with close control of the temperature between 1080°C and 1170°C.

3. Results

3.1. Major element oxide geochemistry

The mafic volcanic lavas at Site 1137 range from evolved basalts to basaltic andesites (Mg# = 0.44–0.58; Table 1) and most are tholeiitic to transitional (alkali index (AI) = −1.9 to 1.1; where negative values are tholeiitic and positive values indicate alkalic compositions [29]). Downcore plots of MgO and TiO_2 wt% and AI show no trends, with the exception of Unit 10, the lowermost basalt unit, which has slightly lower MgO with higher TiO_2 wt% (Fig. 2).

3.2. Alteration

Basalts recovered at Site 1137 show a general positive correlation between weight loss on ignition and total alkali content (wt% Na_2O+K_2O; not shown). Because of post-magmatic alteration, the more mobile incompatible elements including

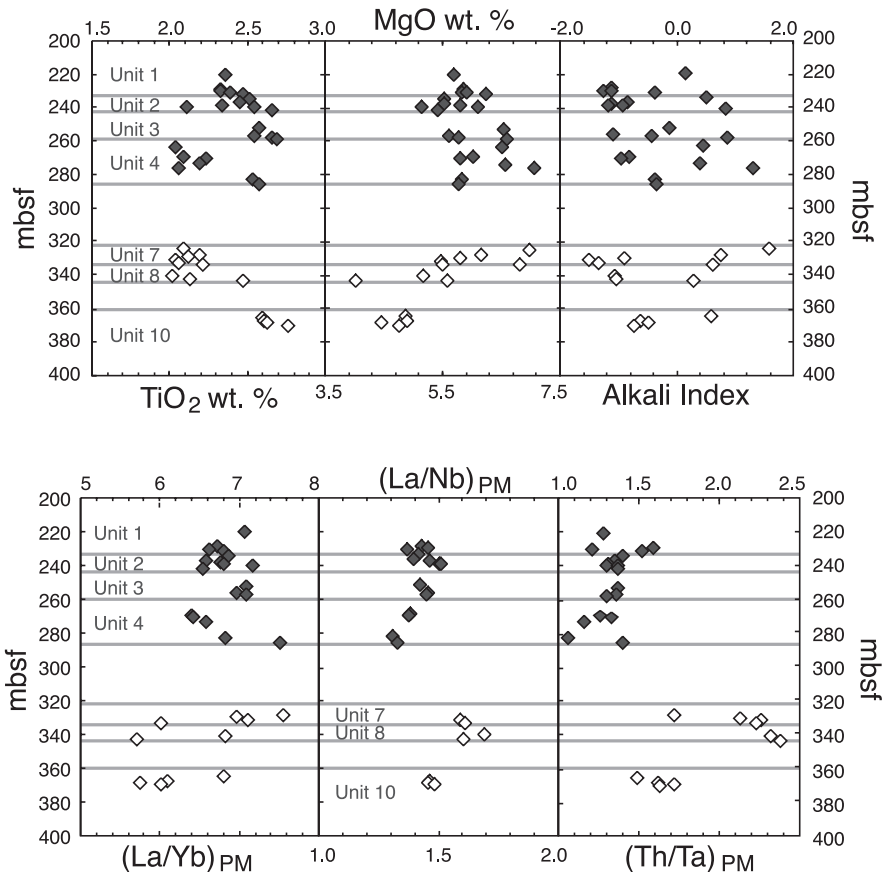

Fig. 2. Geochemical variations downcore of MgO and TiO_2 wt%, alkali index, $(La/Yb)_{PM}$, $(La/Nb)_{PM}$ and $(Th/Ta)_{PM}$ (subscript 'PM' indicates normalization to primitive mantle values [30]) for Site 1137 basalts. The basalts are divided into an upper group (Units 1–4, filled diamonds) and a lower group (Units 7, 8 and 10, open diamonds). The alkali index [29] indicates the relative displacement of a sample from the tholeiitic–alkalic series dividing line; with tholeiitic series rocks having a negative displacement (and a negative alkali index) and alkalic series rocks having a positive displacement (the equation is given as $AI = (Na_2O+K_2O)-(0.37\times SiO_2-14.43)$).

Table 2
Sr, Nd and Pb isotopic ratios in Site 1137 basaltic rocks

Core, Interval	Depth	Unit	$(^{87}Sr/^{86}Sr)_m$	Error	$^{87}Rb/^{86}Sr$	$(^{87}Sr/^{86}Sr)_T$	$(^{143}Nd/^{144}Nd)_m$	Error	$\frac{^{147}Sm}{^{144}Nd}$	$(^{143}Nd/^{144}Nd)_T$	$\varepsilon_{Nd}(T)$	$\frac{^{206}Pb}{^{204}Pb}$	$\frac{^{207}Pb}{^{204}Pb}$	$\frac{^{208}Pb}{^{204}Pb}$
Upper group														
24R-2-10–17	220.39	1	0.705012	7	–	–	0.512553	10	0.148	0.51245	−1.0	18.018	15.620	38.592
25R-1-64–72	229.04	1	0.705005	6	0.0324	0.70496	0.512566	9	0.138	0.51247	−0.6	18.009	15.619	38.567
25R-2-46–53	230.30	1	0.705066	7	0.0655	0.70497	0.512549	10	0.142	0.51245	−1.0	18.018	15.625	38.625
25R-2-119–126	231.03	1	0.704967	6	0.0458	0.70490	0.512559	10	0.136	0.51246	−0.7	17.993	15.616	38.551
25R-7-90–98	237.08	2	0.704987	7	0.0658	0.70489	0.512583	15	0.139	0.51248	−0.3	17.989	15.620	38.575
26R-1-31–43	238.31	2	0.704999	7	0.0718	0.70489	0.512576	8	0.144	0.51247	−0.5	18.016	15.644	38.663
26R-1-143–146	239.43	2	0.705029	6	0.0673	0.70493	0.512555	9	0.142	0.51245	−0.9	17.997	15.617	38.617
26R-2-17–23	239.65	2	0.705092	7	0.115	0.70492	0.512550	9	0.137	0.51245	−0.9	18.002	15.616	38.634
27R-4-57–63	252.49	3	0.704921	5	0.0990	0.70477	0.512565	9	0.142	0.51246	−0.7	18.012	15.623	38.681
28R-3-123–128	256.62	3	0.704920	6	0.0870	0.70479	0.512580	7	0.145	0.51248	−0.4	18.010	15.608	38.603
29R-1-30–37	257.50	3	0.704825	6	0.0337	0.70477	0.512577	9	0.142	0.51248	−0.4	17.995	15.617	38.622
31R-3-5–10	269.65	4	0.704930	6	0.0589	0.70484	0.512563	7	0.140	0.51246	−0.8	18.072	15.635	38.847
31R-3-5–10*	269.65	4	0.704940	8	–	–	0.512546	10	–	–	–	18.066	15.625	38.816
31R-3-85–90	270.45	4	0.704932	6	0.0565	0.70485	0.512566	12	0.143	0.51247	−0.7	18.036	15.630	38.741
32R-6-66–71	282.88	4	0.704885	7	0.0674	0.70478	0.512600	10	0.145	0.51250	0.0	18.015	15.605	38.631
33R-1-53–60	286.03	4	0.704879	6	0.0444	0.70481	0.512565	10	0.140	0.51247	−0.6	18.019	15.608	38.692
Lower group														
38R-3-63–68	329.95	7	0.705625	7	–	–	0.512519	12	0.136	0.51242	−1.5	17.962	15.639	38.887
38R-4-71–77	331.39	7	0.705690	8	0.0984	0.70554	0.512495	11	0.135	0.51240	−1.9	17.974	15.641	38.910
39R-1-101–108	333.21	7	0.705774	7	0.0998	0.70562	0.512488	10	0.139	0.51239	−2.1	18.004	15.662	39.033
40R-1-14–16	337.74	8	0.706098	8	–	–	0.512463	10	–	–	–	17.961	15.667	39.065
40R-3-117–124	340.62	8	0.706256	7	0.229	0.70590	0.512455	10	0.145	0.51235	−2.8	17.999	15.668	39.144
41R-1-3–10	343.03	8	0.706027	7	0.0557	0.70594	0.512461	8	0.142	0.51236	−2.7	17.969	15.665	39.059
45R-3-57–63	364.84	10	0.705650	8	–	–	0.512512	10	0.136	0.51242	−1.6	18.011	15.654	38.946
46R-1-51–56	367.51	10	0.705633	7	0.0832	0.70550	0.512543	13	0.141	0.51244	−1.1	18.006	15.646	38.876
46R-2-7–15	368.54	10	0.705728	7	0.120	0.70554	0.512546	10	0.142	0.51245	−1.0	18.016	15.662	38.931
46R-3-12–18	369.92	10	0.705680	9	0.123	0.70549	0.512541	7	0.149	0.51244	−1.2	18.011	15.658	38.915

Depth is reported in meters below sea floor. * denotes duplicate analysis. Subscript 'm' denotes a measured ratio and 'T' denotes the ratio corrected for 109 Myr of in situ decay [6]. Error reported is the measured mean (2σ). Measured error (2σ) for $^{206}Pb/^{204}Pb$ is 0.014, $^{207}Pb/^{204}Pb$ is 0.016 and $^{208}Pb/^{204}Pb$ is 0.047. Rb and Sr concentrations are by XRF, Sm and Nd are by NA. $\varepsilon_{Nd}(T)$ is calculated using $^{143}Nd/^{144}Nd$ value for CHUR (today) of 0.512638 [31].

Rb, K and Ba do not correlate well with immobile incompatible elements although immobile, incompatible elements (e.g., Zr and Nb) correlate well with each other (Table 1). For this reason, only data on immobile trace elements and isotope data on leached samples are discussed as being relevant to petrogenetic interpretations.

3.3. Trace element geochemistry

Downcore plots of primitive mantle-normalized incompatible trace element ratios (designated by the subscript 'PM' [30]) demonstrate limited, yet important variations between the upper basalt group, Units 1–4, and the lower basalt group, Units 7, 8 and 10 (Fig. 2). The variation of $(La/Yb)_{PM}$ is fairly limited, from 5.5 to 8. All basalts are enriched in incompatible elements overall when compared to values for the primitive mantle [30]. $(La/Nb)_{PM}$ is greater than unity for all samples, but highest for the lower basalt Units 7 and 8; $(Th/Ta)_{PM}$ values show an even stronger distinction between the upper basalt group, which has values between 1 and 1.5, and the lower basalt group, which has significantly higher values, up to 2.5. In Units 3 and 4, $(Th/Ta)_{PM}$ values are the closest to unity, due mainly to the fact that Th is less enriched in these two units (20–30 × primitive mantle) than in Units 1 and 2 (25–35 × primitive mantle) and the lowermost Units 7, 8 and 10 (30–45 × primitive mantle).

3.4. Sr, Nd and Pb isotopic compositions

Sr, Nd and Pb isotopes demonstrate systematic trends downcore (Table 2). Initial $^{87}Sr/^{86}Sr$, at 109 Ma [6], shows limited variation in Units 1–4 ($(^{87}Sr/^{86}Sr)_T = 0.70477–0.70497$). These values are distinctly lower than those of the lower basaltic lava flows, Units 7, 8 and 10 ($(^{87}Sr/^{86}Sr)_T = 0.70549–0.70595$). $\varepsilon_{Nd}(T)$ (calculated from CHUR values of Goldstein et al. [31]) mirrors these downcore trends, where the highest values are found in the upper basaltic flows ($\varepsilon_{Nd}(T) = -1$ to 0) and the lower values are found in the lower basaltic flows ($\varepsilon_{Nd}(T) = -2.8$ to -1). Unit 8 has the highest $(^{87}Sr/^{86}Sr)_T$ and the lowest $\varepsilon_{Nd}(T)$ of all basalt flows. There is no significant downcore variation in $^{206}Pb/^{204}Pb$, but the highest values occur in Unit 4 ($^{206}Pb/^{204}Pb = 18.07$) and the lowest values in Unit 8 ($^{206}Pb/^{204}Pb = 17.96$). For $^{207}Pb/^{204}Pb$, the highest overall values are in the lowermost units; the highest values of $^{208}Pb/^{204}Pb$ are in Unit 8 ($^{208}Pb/^{204}Pb = 39.14$) and the lowest in Unit 1 ($^{208}Pb/^{204}Pb = 38.55$).

The substantial range of $(^{87}Sr/^{86}Sr)_T$ and $\varepsilon_{Nd}(T)$ in the Bunbury and Rajmahal basalt samples [9,11] encompasses that of the Site 1137 basalts (Fig. 3). Rajmahal Group II basalts show two subgroups, Group IIa and IIb; distinctly more radiogenic $(^{87}Sr/^{86}Sr)_T$ and less radiogenic $\varepsilon_{Nd}(T)$ are found in Group IIb. The small range in $(^{87}Sr/^{86}Sr)_T$ and $\varepsilon_{Nd}(T)$ of the Rajmahal Group IIa lavas is enveloped by the Site 1137 basalts. The Bunbury basalt of Western Australia also has two groups that match well with the two major Rajmahal groups [9]. The Bunbury Casuarina group shows minimal evidence for contamination by continental crust (similar to Rajmahal Group I), whereas the Bunbury Gosselin group have Sr and Nd isotopic compositions near the extreme end of the Rajmahal Group IIb [9]. Some basalts from Site 749 on the SKP have Sr and Nd isotopic compositions similar to those of Rajmahal Group I and Bunbury Casuarina basalts.

Isotope plots of $^{207}Pb/^{204}Pb$ and $^{208}Pb/^{204}Pb$ vs. $^{206}Pb/^{204}Pb$ reveal very steep (nearly vertical) trends for Bunbury, Rajmahal, Site 749 and Site 1137 basalts with a $^{206}Pb/^{204}Pb$ value of ~ 18 (Fig. 3). Site 749, Rajmahal Group I and Bunbury Casuarina basalts have the lowest $^{207}Pb/^{204}Pb$ and $^{208}Pb/^{204}Pb$ values. Rajmahal Group IIa and Site 1137 upper group have values beginning within this range and extending slightly higher. Bunbury Gosselin group, Rajmahal Group IIb and Site 1137 lower group have the highest $^{207}Pb/^{204}Pb$ and $^{208}Pb/^{204}Pb$ values (although most Gosselin samples have low $^{208}Pb/^{204}Pb$). Site 738 basalts have distinctly lower $^{206}Pb/^{204}Pb$, higher $^{207}Pb/^{204}Pb$ and similar $^{208}Pb/^{204}Pb$ values. The trend observed for other basalts erupted early on the Kerguelen Plateau (Sites 747 and 750) is very different from that of the above mentioned basalts, forming a shallow slope toward much lower $^{206}Pb/^{204}Pb$, $^{207}Pb/^{204}Pb$ and $^{208}Pb/^{204}Pb$ values ([32]; Fig. 3).

4. Discussion

4.1. Comparison of the petrogenesis of Site 1137 basalts with Cretaceous basalts of Australia and India

Geochemical similarities exist between Cretaceous continental tholeiitic basalts from the eastern Indian and southwestern Australian margins and basalts from the Kerguelen Plateau (e.g., [4,9,11,13]). The basalts at Site 1137 and Site 749 display striking similarities to the Bunbury basalt and the Rajmahal Traps, specifically in Pb–Pb isotope plots (Fig. 3). The Rajmahal Traps and Bunbury basalt have been interpreted as being variably contaminated by continental lithosphere [4,13], continental crust [11,14] or continental upper crust [9] and this variation forms the basis of their division into separate groups [9]. The Site 1137 basalts also show two distinct groups (upper and lower groups), both with geochemical characteristics more in common with the Bunbury Gosselin and Rajmahal Group II than with Bunbury Casuarina or Rajmahal Group I. All Bunbury Gosselin, Rajmahal Group II and Site 1137 basalts have elevated $(La/Nb)_{PM}$, $(La/Ta)_{PM}$, $(La/Th)_{PM}$, $^{87}Sr/^{86}Sr$ and $^{207}Pb/^{204}Pb$. These geochemical characteristics in Bunbury and Rajmahal basalts have been interpreted as representing contamination by continental material, most likely continental crust [9,11]. We suggest that assimilation of variable amounts of continental lithosphere also explains these geochemical characteristics of the Site 1137 basalts.

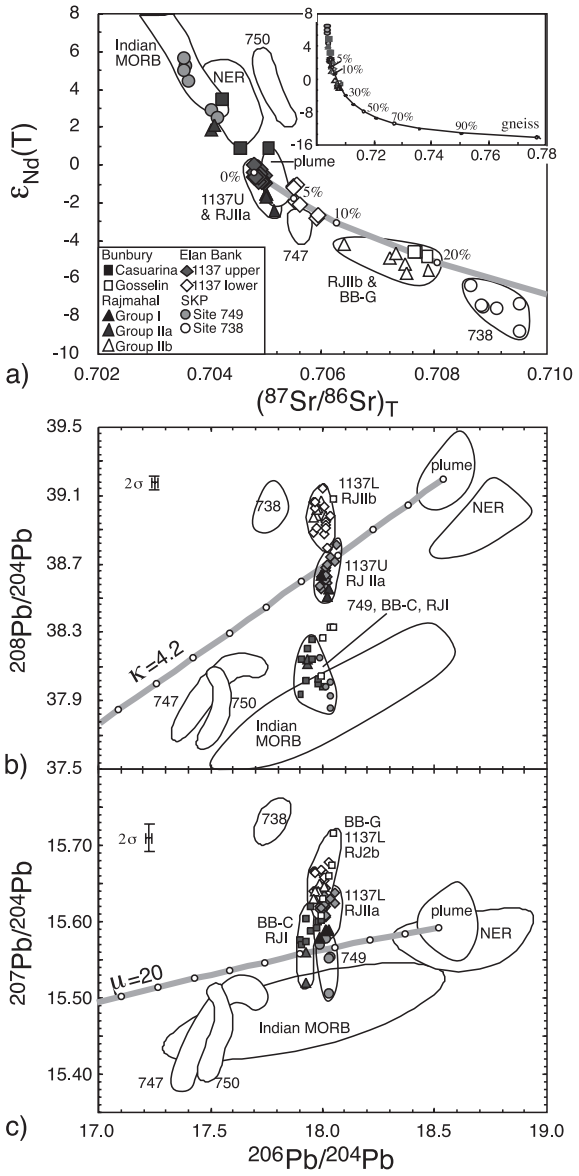

Fig. 3. (a) $\varepsilon_{Nd}(T)$ vs. $(^{87}Sr/^{86}Sr)_T$ for Indian Ocean, Kerguelen Plateau and Eastern Gondwanan continental basalts. Indian MORB data are from [62], Ninetyeast Ridge (NER) data are from [26], Site 738 data are from [4] and values for the Kerguelen plume (labeled 'plume') are from [41]. Bunbury and Rajmahal continental tholeiite data from [9,11], respectively and Kerguelen Plateau data from [32]. The thick gray line represents mixing between a garnet biotite gneiss also recovered in the Site 1137 drill core [19] and the least contaminated basalts from Site 1137. The inset shows the entire mixing line between the Site 1137 basalts and the gneisses (black cross), small white circles are marked with an estimated percentages of assimilation (italicized numbers). $^{208}Pb/^{204}Pb$ vs. $^{206}Pb/^{204}Pb$ (b) and $^{207}Pb/^{204}Pb$ vs. $^{206}Pb/^{204}Pb$ (c) for Indian Ocean, Kerguelen and Eastern Gondwanan continental basalts. 2σ error bars are shown for each figure. The average μ (20) and κ (4.2) have been calculated for basalts considered to be representative of the Kerguelen plume [41]; the thickness of the Pb evolution line represents the inherent uncertainties associated with this calculation. Small white circles are shown for each 50 Myr interval, beginning at the plume field with 0 Myr. Data sources and symbols are the same as in panel a.

4.2. Evidence for assimilation of continental lithosphere

4.2.1. Identification of the continental contaminant

The general characteristics of incompatible trace elements and trends in the isotope diagrams presented above are mostly likely created by the assimilation of continental lithospheric material during ascent of basalt magmas. Distinguishing between the assimilation of subcontinental mantle lithosphere (SCML) and the assimilation of continental crust is a subject of much debate (e.g., [33–35]). McDonough [36] argued that most samples (peridotite xenoliths) from the SCML are not depleted in Nb or Ta; additionally, the SCML also has much lower concentrations of Sr and Nd relative to a plume-derived basalt (e.g., [37]). Thus, contamination by SCML appears unlikely to produce the geochemical characteristics observed in the Site 1137 lower basalt group. Furthermore, as samples of unequivocal continental crust crop out within the Site 1137 core [5], these crust samples are the most conspicuous contaminant for the Site 1137 basalts. The garnet–biotite gneiss has very high abundances of La, Th, Pb and Nd, very high $^{87}Sr/^{86}Sr$ values and very low concentrations of Nb and Ta [19], comparable to the geochemical characteristics of continental crust [38,39].

Increasing SiO_2 wt% (or decreasing MgO wt%) in combination with increasing radiogenic isotope ratios characteristically enriched in the continental crust (e.g., $^{87}Sr/^{86}Sr$, $^{207}Pb/^{204}Pb$ or $^{208}Pb/^{204}Pb$) is indicative of assimilation of continental crust by basaltic magmas (e.g., [40]). Although these trends are recognized in the Rajmahal Traps lavas, Site 1137 upper and lower basalt groups span a similar range in SiO_2 wt% and are only distinguished by the more radiogenic $^{87}Sr/^{86}Sr$ of the lower basalt group (Fig. 4). We interpret this to indicate that the Site 1137 basalts did not assimilate enough continental crust to have affected their major element concentrations and that the lower basalt group is more contaminated than the upper basalt group.

Continental crust is typically highly depleted in elements such as Ta and Nb [39]. Upper continental crust is enriched in La and Th while lower continental crust is not usually enriched in Th [38]. The Site 1137 basalts, in addition to those of Site 749, Rajmahal and Bunbury, follow a trend toward upper continental crust in a plot of $(Th/Ta)_{PM}$ vs. $(La/Ta)_{PM}$ (Fig. 4). All samples define a line that could represent mixing between

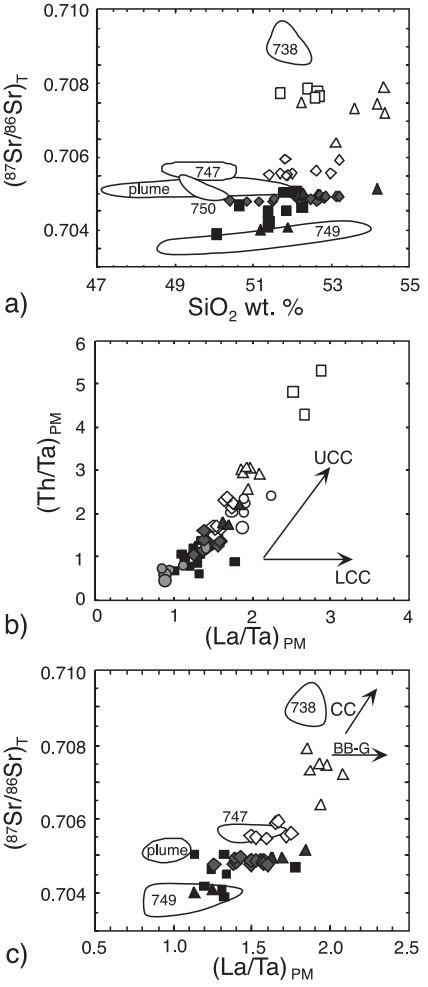

Fig. 4. (a) Variation of $(^{87}Sr/^{86}Sr)_T$ vs. SiO_2 wt% for basalts associated temporally and spatially with the early Kerguelen plume. (b) $(Th/Ta)_{PM}$ vs. $(La/Ta)_{PM}$ for the same basalts as in panel a. Arrows indicate typical vectors created by assimilation of upper continental crust (UCC) and lower continental crust (LCC). (c) $(^{87}Sr/^{86}Sr)_T$ vs. $(La/Ta)_{PM}$ for the same basalts as in panel a. The arrow points in the direction of typical continental crust, which is generally enriched in $^{87}Sr/^{86}Sr$ and La relative to Ta [37,38]. Bunbury Gosselin basalts fall outside the plot perimeter toward much higher $(La/Ta)_{PM}$ values. Data sources and symbols are the same as in Fig. 3.

mantle melts and upper continental crust, except for a few Bunbury Casuarina samples. Additionally, contamination by upper continental crust would readily explain an increase in $^{87}Sr/^{86}Sr$ coupled with an increase in $(La/Ta)_{PM}$ (Fig. 4).

4.2.2. Quantification of the continental contaminant

For the mantle endmember of the calculation, we use the least contaminated basalt samples from the Site 1137 core. Unit 4 of the upper basalt group has the lowest $^{207}Pb/^{204}Pb$, $^{208}Pb/^{204}Pb$, $(^{87}Sr/^{86}Sr)_T$, the highest $\varepsilon_{Nd}(T)$ and La/Nb, La/Ta and La/Th closest to primitive mantle values. These general characteristics suggest that contamination is minimal in Unit 4 basalts and that their composition may best approximate the Kerguelen plume at the time of eruption of the Site 1137 basalts. The evolution of the Kerguelen plume Pb isotopic composition is estimated based on a μ ($^{238}U/^{204}Pb$) of 20 and κ ($^{232}Th/^{238}U$) of 4.2 (Fig. 3; calculated on the basis of average compositions considered to be representative of the Kerguelen plume [41]). These values are similar to those of Lassiter et al. [42], calculated on the basis of average Kerguelen Islands data from Sun and McDonough [30]. The Kerguelen plume would intersect with the least contaminated basalts of Site 1137 around 150 Ma; thus, it is a reasonable assumption that these basalts record the Kerguelen plume composition. Additionally, the Kerguelen plume appears to be an appropriate mantle source for the Bunbury and Rajmahal basalts. However, because the Bunbury Casuarina, Rajmahal Group I and Site 749 basalts plot below the Pb evolution curve of the Kerguelen plume; we thus infer an additional, depleted mantle component in their source.

The composition of the continent-derived gneiss clasts can be used as the potential contaminant in the Site 1137 basalts. These gneiss clasts have an isotopic composition similar to rocks of the Eastern Ghats Belt, a Paleoproterozoic terrane in eastern India [19,43]. For both Sr and Nd isotopes, using the equations of Vollmer [44] we obtain independently consistent results. A calculation assuming endmembers of the least contaminated Site 1137 basalt and the gneiss clast requires approximately 9% of the garnet–biotite gneiss to be assimilated by the basaltic magmas in order to reach the composition of the most contaminated basalts (Fig. 3). Pb isotopic systematics are more difficult to explain because the $^{206}Pb/^{204}Pb$ remains fairly constant from the least contaminated basalt to the most. Unfortunately no Pb concentration data is available for the basalts, but using various estimations for Pb concentrations in tholeiitic basalts (from 1 to 5 ppm), both the $^{207}Pb/^{204}Pb$ and the $^{208}Pb/^{204}Pb$ yield consistent results for the amount of contaminant required to explain the data ($\sim$5%), however the quantity of contamination required is somewhat less than that required to explain the Sr–Nd systematics.

The above estimates on the percent assimilate are based on simple bulk mixing equations. When we combine the effects of assimilation and fractional crystallization, we can more rigorously constrain the amount of assimilate to original magma. We use the equations of DePaolo [45] and estimate the rate of assimilation to fractional crystallization using graphical interpolations as demonstrated by Aitcheson and Forrest [46]; this results in a rate of assimilation to rate of fractional crystallization (r) of 0.1. Using this more realistic approach than bulk mixing, the fraction of contaminating gneiss is calculated to be between 6.5 and 7% for the most contaminated basalts (Unit 8). This is essentially in the same range as the bulk mixing prediction, especially if the errors associated with calculating the bulk solid/melt partition coefficients for Sr and Nd concentrations in basaltic rocks are taken into account. Therefore, we place the upper limit on the amount of crustal contamination as $\sim$7%, based on the results calculated using Sr and Nd concentrations and isotopes, and the lower limit at 5%, based on the results of the Pb isotope systematics. Alternatively, if a depleted mantle source is considered (rather than an enriched, plume-like source), attempts at quantification of the contaminant yield highly inconsistent results. For example, the small shifts in Sr isotopic composition would require only a few percent assimilate while the huge shifts in Nd isotopes would require vastly greater quantities of contaminating material, as much as an order of magnitude more.

4.3. Tectonic and age constraints for the involvement of the Kerguelen plume in the Bunbury, Rajmahal and Kerguelen Plateau basalts

It would be relatively straightforward to explain the common geochemical characteristics between continental basalts of the eastern Indian and southwestern Australian margins and those of the Kerguelen Plateau were the Kerguelen plume implicated in the breakup of India, Australia and Antarctica (Fig. 5). If the early Cretaceous Bunbury, Rajmahal and Site 1137 basalts were derived from the Kerguelen plume, they represent ~23 Myr of volcanic activity. All of these basalts post-date the oldest known magnetic anomalies in the Indian Ocean which lie off the northwest coast of Australia [47], and this makes their geochemical similarities somewhat difficult to reconcile. Magnetic anomalies as old as M25 (~154 Ma) occur off the northwestern coast of Australia.

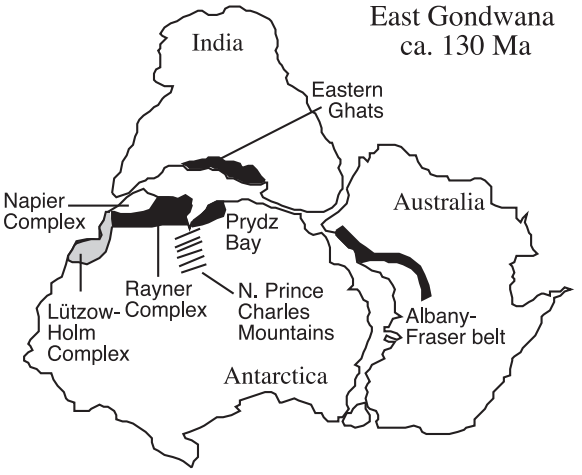

Fig. 5. Generalized plate tectonic reconstruction prior to complete breakup between West Australia, East Antarctica and eastern Greater India ca. 130 Ma (after [48,60]). The major Proterozoic mobile belts are indicated (locations from [63]). The gneiss clasts recovered from Site 1137 used to model the crustal contaminant in the basalt flows may originate from the Eastern Ghats Belt [19]. Elan Bank may be a microcontinent splintered from the eastern margin of India through interaction of the Kerguelen plume with the newly formed margin (e.g., [8,19,61]).

However, magnetic anomalies get younger to the south along the western coast of Australia and nearest the location of the Bunbury basalt, the oldest anomalies are M10N (~132 Ma; magnetic anomalies reported by Royer and Coffin [48] and ages from the time scale of Gradstein et al. [49]). This implies that the separation between northern India and West Australia may have proceeded as an unzipping from north to south over a time interval spanning more than 20 Myr. Alternatively, Müller et al. [50] proposed that separation proceeded by transform motion within Greater India, the northern half moving away from Australia before the southern half. The separation between eastern India and East Antarctica is less well constrained. Müller et al. [50] demonstrated that breakup must have occurred later than 120 Ma while previous reconstructions have placed it near 130 Ma [51]. Most recently, Coffin et al. [8] suggest that eastern India was fairly well separated from both southwestern Australia and eastern Antarctica by about 130 Ma. To further explore the tectonic setting of the early Kerguelen plume, we propose two possibilities:

1. *Post-breakup oceanic plume*. In this scenario, the initial magmatism related to the Kerguelen plume took place well after continental rifting, and the initial Kerguelen Plateau was constructed in the Indian Ocean basin. Geochemical similarities between the Casuarina group of Bunbury, Rajmahal Group I and Site 749 and between the Gosselin group of Bunbury, Rajmahal Group II and Site 1137 would, in this case, be coincidental. Here, the 130–123 Ma Bunbury basalt is associated with the prolonged stretching phase of continental breakup, i.e., they represent small amounts of volcanism typical of non-volcanic rifted margins (e.g., [52]). The unusually limited variation in $^{206}Pb/^{204}Pb$ of the Bunbury, Rajmahal and some Kerguelen basalts would be difficult to reconcile in this scenario, especially if the higher $^{207}Pb/^{204}Pb$ and $^{208}Pb/^{204}Pb$ result from contamination by continental crust, which tends to be very heterogeneous. Duncan [7] proposes that the entire Kerguelen Plateau may have formed around 118 Ma (adhering to the decompressing plume head model [53]) and that

younger volcanism (e.g., Site 1137) represents small volume magmatism from the Kerguelen plume tail as the Kerguelen Plateau migrated south relative to the fixed hotspot. These younger magmas could have assimilated material from the overlying ($\sim$118 Ma) plateau crust, but this is difficult to assess geochemically.

2. *Pre-breakup or breakup plume*. Storey et al. [22] proposed that the Kerguelen plume was present prior to continental rifting and Kent [23] advocated a long-term, incubating plume head prior to continental breakup. If so, then the geochemical similarities between Bunbury, Rajmahal and Kerguelen basalts would reflect a common origin by partial melting of similarly geochemically characterized mantle material contaminated by similarly-aged continental crust. However, the reportedly small volume of the Bunbury basalt ($\sim 10^3$ km^3 [8]) is significantly lower than that typically associated with plume-related continental flood basalt volcanism ($\sim 10^5$–10^6 km^3 [54]). Coffin et al. [8] suggested that the initial Kerguelen plume head might have broken into 'droplets' of variable sizes within the rapidly convecting upper mantle, resulting in spatially and temporally displaced magmatic events of differing volumes, all ultimately related to the Kerguelen plume.

The second model best explains the geochemical similarities between Bunbury, Rajmahal, Site 749 and Site 1137 basalts. The plume source would be readily available for these different basalt groups. The geochemical variations could then be explained by crust contamination and/or an additional depleted component (required to explain the group including the Bunbury Casuarina, Rajmahal Group I and Site 749 basalts). However, at this time, we cannot explain why continental flood basalt volcanism does not appear to pre-date the rifting, as is typical of areas where plumes are present prior to the onset of rifting (e.g., [55]). Nevertheless, it appears clear that the Kerguelen plume did interact with the continental margins of eastern India and western Australia and was involved with isolating microcontinents from their margins [8,19,50].

5. Conclusions

Geochemical similarities between select early Cretaceous basalts of the Indian Ocean and Kerguelen Plateau indicate two broad groups, based on basalt geochemistry: the first group includes the Bunbury Casuarina group, the Rajmahal Group I and Site 749 on the Southern Kerguelen Plateau and the second group includes the Bunbury Gosselin group, the Rajmahal Group II and Site 1137. Although these basalts are presently located several thousand kilometers apart, when they erupted they were separated by less than 1000 km. Both the geochemical data and plate tectonic reconstructions are permissive of an origin for both groups from the Kerguelen plume. However, the first group requires some input from depleted asthenospheric mantle, while in the second group, no depleted component is required. Site 1137 basalts show evidence for contamination by continental crust as has been previously suggested for the Bunbury basalt and Rajmahal Traps [9,11]. In Site 1137 basalts, assimilation of as much as 7% of upper crustal material is required to explain the compositions of the most contaminated basalts.

Until the timing of rifting between Australia, India and Antarctica is better constrained, we cannot ascertain if the Kerguelen plume played a causal role during the early stages of continental rifting. It remains possible that the arrival of the Kerguelen plume in an already rifting environment was fortuitous. Increasingly, however, geochemical and geophysical evidence requires the presence of a mechanism which aided in the isolation of fragments of continental crust at shallow levels in the early Indian Ocean basin during the early rifting stages of Eastern Gondwana. The Kerguelen plume may have been present during early rifting activity but not necessarily the driving force behind the opening of the Indian Ocean.

Acknowledgements

Thanks go to G. Brügmann, M. Coffin, D. Damasceno, R. Kent, and N. Mattielli, for dis-

cussions that improved some of the ideas presented here. A. Saunders and A. le Roex are greatly thanked for providing critical reviews. C. Maerschalk is thanked for his help in the laboratory. We thank M. Rhodes and the University of Massachusetts for X-ray fluorescence analyses. Dr. P. Ila is thanked for supervision of the INAA facility at MIT. The first author is supported by, and the work presented here is funded by an ARC grant (#03/233) from the Communauté française de Belgique. The Fonds National de la Recherche Scientifique funds Belgian membership in the Ocean Drilling Program (ODP) and supported the second author's participation in ODP Leg 183, where sampling was carried out (F.N.R.S. Grant 3.4579.99). The ODP is sponsored by the U.S. National Science Foundation and participating member countries under the management of Joint Oceanographic Institutions, Inc. Additional funding for this research was provided by the U.S. Science Support Program (USSSP).*[BOYLE]*

References

[1] M.F. Coffin, O. Eldholm, Large igneous provinces: crustal structure, dimensions, and external consequences, Rev. Geophys. 32 (1994) 1–36.

[2] H.L. Davies, S.-s. Sun, F.A. Frey, I. Gautier, M.T. McCulloch, R.C. Price, Y. Bassias, C.T. Klootwijk, L. Leclaire, Basalt basement from the Kerguelen Plateau and the trail of a Dupal plume, Contrib. Mineral. Petrol. 103 (1989) 457–469.

[3] D. Weis, Y. Bassias, I. Gautier, J.-P. Mennessier, Dupal anomaly in existence 115 Ma ago: evidence from isotopic study of the Kerguelen Plateau (South Indian Ocean), Geochim. Cosmochim. Acta 53 (1989) 2125–2131.

[4] J.J. Mahoney, W.B. Jones, F.A. Frey, V.J.M. Salters, D.G. Pyle, H.L. Davies, Geochemical characteristics of lavas from Broken Ridge, the Naturaliste Plateau and southernmost Kerguelen Plateau: Cretaceous plateau volcanism in the southeast Indian Ocean, Chem. Geol. 120 (1995) 315–345.

[5] F.A. Frey, M.F. Coffin, P.J. Wallace, D. Weis, X. Zhao, S.W. Wise Jr., V. Wähnert, D.A.H. Teagle, P.J. Saccocia, D.N. Reusch, M.S. Pringle, K.E. Nicolaysen, C.R. Neal, R.D. Müller, C.L. Moore, J.J. Mahoney, L. Keszthelyi, H. Inokuchi, R.A. Duncan, H. Delius, J.E. Damuth, D. Damasceno, H.K. Coxall, M.K. Borre, F. Boehm, J. Barling, N.T. Arndt, M. Antretter, Origin and evolution of a submarine large igneous province: the Kerguelen Plateau and Broken Ridge, southern Indian Ocean, Earth Planet. Sci. Lett. 176 (2000) 73–89.

[6] M.S. Pringle, R.A. Duncan, Basement ages from the Southern and Central Kerguelen Plateau: initial products of the Kerguelen Large Igneous Province, EOS Trans. Am. Geophys. Union 81 (2000) 424.

[7] R.A. Duncan, A timeframe for construction of the Kerguelen Plateau and Broken Ridge, J. Petrol. (in press).

[8] M.F. Coffin, M.S. Pringle, R.A. Duncan, T.P. Gladczenko, M. Storey, Kerguelen hot spot magma output since 130 Ma, J. Petrol. (in press).

[9] F.A. Frey, N.J. McNaughton, D.R. Nelson, J.R. deLaeter, R.A. Duncan, Petrogenesis of the Bunbury Basalt, Western Australia: interaction between the Kerguelen plume and Gondwana lithosphere?, Earth Planet. Sci. Lett. 144 (1996) 163–183.

[10] A.K. Baksi, Petrogenesis and timing of volcanism in the Rajmahal flood basalt province, northeastern India, Chem. Geol. 121 (1995) 73–90.

[11] R.W. Kent, A.D. Saunders, P.D. Kempton, N.C. Ghose, Rajmahal Basalts, Eastern India: mantle sources and melt distribution at a volcanic rifted margin, in: M. Coffin, J. Mahoney (Eds.), Large Igneous Provinces: Continental, Oceanic, and Planetary Flood Volcanism, Am. Geophys. Union Geophys. Monogr. 100 (1997) 145–182.

[12] R.W. Kent, M.S. Pringle, R.D. Müller, A.D. Saunders, N.C. Ghose, $^{40}Ar/^{39}Ar$ geochronology of the Rajmahal basalts, India, and their relationship to the Kerguelen Plateau, J. Petrol. (in press).

[13] M. Storey, R.W. Kent, A.D. Saunders, V.J.M. Salters, J. Hergt, H. Whitechurch, J.H. Sevigny, M.F. Thirlwall, P. Leat, N.C. Ghose, M. Gifford, Lower Cretaceous volcanic rocks on continental margins and rheir relationship to the Kerguelen Plateau, in: W.S. Wise, R. Schlich et al., Proc. ODP Sci. Results 120, 33–47.

[14] J.J. Mahoney, J.D. Macdougall, G.W. Lugmair, K. Gopalan, Kerguelen hotspot source for Rajmahal Traps and Ninetyeast Ridge?, Nature 303 (1983) 385–389.

[15] P. Charvis, S. Operto, O. Lesne, J. Royer, Velocity structure of the Kerguelen volcanic province from wide-angle seismic data: Petrological implications, EOS Trans. Am. Geophys. Union 78 (1997) 711.

[16] I. Borissova, A. Moore, J. Sayers, P. Symonds, I. Teliatnikov, Volcanostratigraphy of the Elan Bank (Kerguelen Plateau) and implications for regional tectonics, EOS Trans. Am. Geophys. Union 81 (2000) 431.

[17] Shipboard Scientific Party, in: M.F. Coffin, F.A. Frey, P.J. Wallace et al., Site 1137, Proc. ODP Init. Reports 183 (2000) 1–102 [CD-ROM].

[18] K. Nicolaysen, S. Bowring, F.A. Frey, D. Weis, S. Ingle, M.S. Pringle, M.F. Coffin, the Leg 183 Shipboard Scientific Party, Provenance of Proterozoic garnet-biotite gneiss recovered from Elan Bank, Kerguelen Plateau, southern Indian Ocean, Geology 29 (2001) 235–238.

[19] S. Ingle, D. Weis, F.A. Frey, Indian continental crust sampled as pebbles within Elan Bank, Kerguelen Plateau (ODP Leg 183, Site 1137), J. Petrol. (in press).

[20] D. Weis, S. Ingle, D. Damasceno, F.A. Frey, K. Nicolaysen, J. Barling, the Leg 183 Shipboard Scientific Party Party, Origin of continental components in Indian Ocean basalts evidence from Elan Bank (Kerguelen Plateau, ODP Leg 183, Site 1137), Geology 29 (2001) 147–150.
[21] R.D. Müller, J.-Y. Royer, L.A. Lawver, Revised plate motions relative to the hotspots from combined Atlantic and Indian Ocean hotspot tracks, Geology 21 (1993) 275–278.
[22] M. Storey, A.D. Saunders, J. Tarney, I.L. Gibson, M.J. Norry, M.F. Thirlwall, P. Leat, R.N. Thompson, M.A. Menzies, Contamination of Indian Ocean asthenosphere by the Kerguelen–Heard mantle plume, Nature 338 (1989) 574–576.
[23] R. Kent, Lithospheric uplift in eastern Gondwana: evidence for a long-lived mantle plume system?, Geology 19 (1991) 19–23.
[24] F.A. Frey, W.B. Jones, H. Davies, D. Weis, Geochemical and petrologic data for basalts from Sites 756, 757, and 758: implications for the origin and evolution of Ninetyeast Ridge, in: J. Weissel, J. Peirce, J. Alt et al., Proc. ODP 121 (1991) 611–659.
[25] J.J. Mahoney, An isotopic survey of Pacific oceanic plateaus: implications for their nature and origin, in: B.H. Keating, P. Fryer, R. Batiza, G.W. Boehlert. (Eds.), Seamounts, Islands, and Atolls, Am. Geophys. Union Geophys. Monogr. 43 (1987) 207–220.
[26] D. Weis, F.A. Frey, Isotope geochemistry of the Ninetyeast Ridge basement basalts: Sr, Nd, and Pb evidence for involvement of the Kerguelen Hot Spot, in: J. Weissel, J. Peirce, J. Alt et al., Proc. ODP 121 (1991) 591–610.
[27] D. Weis, D. Demaiffe, S. Cauët, M. Javoy, Sr, Nd, O and H isotopic ratios in Ascension lavas and plutonic inclusions: cogenetic origin, Earth Planet. Sci. Lett. 82 (1987) 316–322.
[28] C. Chauvel, J. Blichert-Toft, A hafnium isotope and trace element perspective on melting of the depleted mantle, Earth Planet. Sci. Lett. 190 (2001) 137–151.
[29] I.S.E. Charmichael, F.J. Turner, F. Verhoogen, Igneous Petrology, McGraw-Hill, New York, 1974, 739 pp.
[30] S.-s. Sun, W.F. McDonough, Chemical and isotopic systematics of oceanic basalts: implications for mantle composition and processes, in: A. Saunders, M. Norry (Eds.), Magmatism in the Ocean Basins, Geol. Soc. London Spec. Publ. 42 (1989) 313–345.
[31] S.L. Goldstein, R.K. O'Nions, M.A. Hamilton, A Sm–Nd isotopic study of atmospheric dusts and particulates from major river systems, Earth Planet. Sci. Lett. 70 (1984) 221–226.
[32] F.A. Frey, D. Weis, A.Yu. Borisova, G. Xu, Involvement of continental crust in formation of the Kerguelen Plateau: new perspectives from ODP Leg 120 Sites, J. Petrol. (in press).
[33] C.J. Hawkesworth, P.D. Kempton, N.W. Rogers, R.M. Ellam, P.W. vanCalsteren, Continental mantle lithosphere, and shallow level enrichment processes in the Earth's mantle, Earth Planet. Sci. Lett. 96 (1990) 256–268.
[34] N.T. Arndt, U. Christensen, The role of lithospheric mantle in continental flood volcanism: thermal and geochemical constraints, J. Geophys. Res. 97 (1992) 10967–10981.
[35] D.J. DePaolo, E.E. Daley, Neodymium isotopes in basalts of the southwest basin and range and lithospheric thinning during continental extension, Chem. Geol. 169 (2000) 157–185.
[36] W.F. McDonough, Constraints on the composition of the continental lithospheric mantle, Earth Planet. Sci. Lett. 101 (1990) 1–18.
[37] D.W. Peate, C.J. Hawkesworth, M.S.M. Mantovani, N.W. Rogers, S.P. Turner, Petrogenesis and stratigraphy of the high-Ti/Y Urubici magma type in the Parana Flood Basalt Province and implications for the nature of 'Dupal'-type mantle in the South Atlantic Region, J. Petrol. 40 (1999) 451–473.
[38] R.L. Rudnick, D.M. Fountain, Nature and composition of the continental crust: A lower crustal perspective, Rev. Geophys. 33 (1995) 267–309.
[39] M.G. Barth, W.F. McDonough, R.L. Rudnick, Tracking the budget of Nb and Ta in the continental crust, Chem. Geol. 165 (2000) 197–213.
[40] G. Rogers, R. Macdonald, J.G. Fitton, R. George, M. Smith, B. Barreiro, Two mantle plumes beneath the East African rift system: Sr, Nd and Pb isotope evidence from Kenya Rift basalts, Earth Planet. Sci. Lett. 176 (2000) 387–400.
[41] D. Weis, F.A. Frey, R. Schlich, M. Schaming, R. Montigny, D. Damasceno, N. Mattielli, K. Nicolaysen, J.S. Scoates, Trace of the Kerguelen mantle plume from seamounts between the Kerguelen Archipelago and Heard Island, Indian Ocean, Geochem. Geophys. Geosyst. in press.
[42] J.C. Lassiter, D.J. DePaolo, J.J. Mahoney, Geochemistry of the Wrangellia flood basalt province: implications for the role of continental and oceanic lithosphere in flood basalt genesis, J. Petrol. 36 (1995) 983–1009.
[43] K. Rickers, K. Mezger, M.M. Raith, Evolution of the continental crust in the Proterozoic Eastern Ghats Belt, India and new constraints for Rodinia reconstruction: implications from Sm-Nd, Rb-Sr and Pb-Pb isotopes, Precambrian Res. 112 (2001) 183–210.
[44] R. Vollmer, Rb-Sr and U-Th-Pb systematics of alkaline rocks: the alkaline rocks from Italy, Geochim. Cosmochim. Acta 40 (1976) 283–295.
[45] D.J. DePaolo, Trace element and isotopic effects of combined wallrock assimilation and fractional crystallization, Earth Planet. Sci. Lett. 53 (1981) 189–202.
[46] S.J. Aitcheson, A.H. Forrest, Quantification of crustal contamination in open magmatic systems, J. Petrol. 35 (1994) 461–488.
[47] J.J. Veevers, Z.X. Li, Review of seafloor spreading around Australia, Aust. J. Earth Sci. 38 (1991) 291–408.
[48] J.-Y. Royer, M.F. Coffin, Jurassic to Eocene plate tectonic reconstructions in the Kerguelen Plateau region, in: W.S. Wise, R. Schlich et al., Proc. ODP Sci. Results 120 (1992) 917–928.

[49] F.M. Gradstein, F.P. Agterberg, J.G. Ogg, J. Hardenbol, P. van Veen, J. Thierry, Z. Huang, A Mesozoic time scale, J. Geophys. Res. 99 (1994) 24051–24074.
[50] R.D. Müller, C. Gaina, A.A. Tikku, D. Mihut, S.C. Cande, J.M. Stock, Mesozoic/Cenozoic tectonic events around Australia, in: M.A. Richards, R.G. Gordon, R.D. van der Hilst (Eds.), The History and Dynamics of Global Plate Motion, Am. Geophys. Union Geophys. Monogr. 121 (2000) 161–188.
[51] L. Lawver, L. Gahagan, M. Coffin, The development of paleoseaways around Antarctica, in: J.P. Kennett, D.A. Warnke (Eds.), The Antarctic Paleoenvironment: A Perspective on Global Change, Am. Geophys. Union Antarct. Res. Ser. 56 (1992) 7–30.
[52] R.S. White, Magmatism during and after continental break-up, in: B. Storey, T. Alabaster, R. Pankhurst (Eds.), Magmatism and the Causes of Continental Break-up, Geol. Soc. Am. Spec. Publ. 68 (1992) 1–16.
[53] I.H. Campbell, R.W. Griffiths, Implications of mantle plume structure for the evolution of flood basalts, Earth Planet. Sci. Lett. 99 (1990) 79–93.
[54] R.L. Larson, Geological consequences of superplumes, Geology 19 (1991) 963–966.
[55] K. Gallagher, C.J. Hawkesworth, Dehydration melting and the generation of continental flood basalts, Nature 258 (1992) 57–59.
[56] Shipboard Scientific Party, in: M.F. Coffin, F.A. Frey, P.J. Wallace et al., Leg 183 Summary: Kerguelen Plateau–Broken Ridge – A large igneous province, Proc. ODP Init. Reports 183 (2000) 1–101.
[57] D. Weis, F.A. Frey, A. Giret, J.-M. Cantagrel, Geochemical characteristics of the youngest volcano (Mount Ross) in the Kerguelen Archipelago: inferences for magma flux, lithosphere assimilation and composition of the Kerguelen Plume, J. Petrol. 39 (1998) 973–994.
[58] H.-J. Yang, F.A. Frey, D. Weis, A. Giret, D. Pyle, G. Michon, Petrogenesis of the flood basalts forming the Northern Kerguelen Archipelago: implications for the Kerguelen Plume, J. Petrol. 39 (1998) 711–748.
[59] K. Nicolaysen, F.A. Frey, K.V. Hodges, D. Weis, A. Giret, $^{40}Ar/^{39}Ar$ geochronology of flood basalts from the Kerguelen Archipelago, southern Indian Ocean: implications for Cenozoic eruption rates of the Kerguelen plume, Earth Planet. Sci. Lett. 174 (2000) 313–328.
[60] Z.X. Li, C.M. Powell, An outline of the palaeogeographic evolution of the Australasian region since the beginning of the Neoproterozoic, Earth Sci. Rev. 53 (2001) 237–277.
[61] T.P. Gladczenko, M.F. Coffin, Kerguelen Plateau crustal structure and basin formation from seismic and gravity data, J. Geophys. Res. 106 (2001) 16583–16601.
[62] J. Mahoney, A.P. le Roex, Z. Peng, R.L. Fisher, J.H. Natland, Southwestern limits of Indian Ocean Ridge mantle and the origin of low $^{206}Pb/^{204}Pb$ mid-ocean ridge basalt: isotope systematics of the Central and Southwest Indian Ridge (17°–50°E), J. Geophys. Res. 97 (1992) 19,771–19,790.
[63] S.D. Boger, C.J. Carson, C.J.L. Wilson, C.M. Fanning, Neoproterozoic deformation in the Radok lake region of the northern Prince Charles Mountains, east Antarctica; evidence for a single protracted orogenic event, Precambrian Res. 104 (2000) 1–24.